

Characterization of Ba(Zr-Ti)O₂ Semiconductors Prepared by Solid State Process

¹Saber E. Mansour, ¹Osama A. Desouky, ³El-Sayed M. Negim,

²Adel M. Najar, ⁴A.A. Shaikhudinova and ⁴G. Zh. Yelighbayeva

¹Department of Chemistry, Faculty of Science,

Omar Al-Mukhtar University, Box 919, Al-Bayda, Libya

²Department of Chemistry, Faculty of Education, University of Benghazi, Benghazi, Libya

³Faculty of Science and Engineering, University of Wolverhampton,

Wulfruna Street, Wolverhampton, West Midlands, WV1 1LY, UK

⁴K.I. Satpaev Kazakh National Technical University22,

Satpaevavenue, Almaty, 050013, Kazakhstan

Abstract: ZrO₂ and TiO₂ substituted BaO semiconductor samples are prepared by using the well-known solid-state reaction method. The considered samples are investigated for phase purity and grain morphology by using X-ray diffraction (XRD) and scanning electron microscope (SEM). While current-voltage (I-V) characteristics are obtained from dc electrical measurements, (I-V) characteristics of different mixes exhibit ohmic relation. RCL circuit was used to measure the capacitance and resistance at different frequencies and constant temperature (25°C). The dielectric constant and conductivity were calculated. The change in resistivity with frequency was followed up to 100kHz. More generally the capacitances in pf for all samples decrease with increasing frequency.

Key words: BaO • ZnO • TiO₂ • Semiconductors • X-ray diffraction • SEM • Electrical properties • Microstructure

INTRODUCTION

Titanium (IV) oxide or titania (TiO₂) exhibits unusual structural, optical, electronic, magnetic and chemical properties [1, 2]. As a consequence, it has found wide applications in pigment [3], photo catalysts [4], solar cells [5], ceramics [6], inorganic membranes [7], sensors [8], nonlinear optics [9] and environmental purification [8]. Titania can also be employed for splitting of water, based on the principles of photo-electrochemistry [10].

Barium titanate zirconium Ba(Ti_{1-x}Zr_x)O₃ (BTZ) ceramics, based on a solid solution of BaZrO₃ and BaTiO₃, have been widely studied and adapted to meet the Y5V and Z5U specifications of multilayer ceramic capacitors, owing to their very high and broad relative permittivity maximum at the ferroelectric Curie temperature (*T_C*) [14, 15]. Owing to the solid-state reaction during sintering, the sintering temperature of BTZ ceramics is always above 1350°C [16]. Recently, Ba (Zr_xTi_{1-x})O (BZT) has been

suggested as an alternative to BST in the fabrication of ceramic capacitors because Zr⁴⁺ is chemically more stable than Ti⁴⁺ [17-19]. The fabrication of BZT thin films by sol-gel method [20], rf-magnetron sputtering [21] and pulsed laser disposition (PLD) [22] and their dielectric properties have been reported recently.

The crystal phase with the structure BaZn₂Ti₄O₁₁ exists in various commercial microwave (MW) dielectric materials based on barium poly titanates (BaTi₄O₉ and Ba₂Ti₉O₂₀) doped with zinc, niobium and tantalum oxides [23, 24]. The BaZn₂Ti₄O₁₁ phase was synthesized for the first time by Gornikov *et al.* [25] using a high-temperature interaction between barium tetra titanate (BaTi₄O₉) and zinc oxide (ZnO). He calculated the crystallographic parameters of the new compound and determined its composition as Ba₃ Zn₇ Ti₁₂ O₃₄ (3BaTi₄O₉ × 7ZnO). This formula (Ba₃Zn₇Ti₁₂O₃₄) was used for many years by various authors when referring to the phase content of ceramics based on doped

barium polytitanates [24-26]. More recently, Roth *et al.*, [27] suggested the phase diagram of the ternary system BaOZnO-TiO₂ and reported the chemical composition of the compound BaZn₂Ti₄O₁₁, with the ratio of the starting oxides being close to 1:2:4. Ti atoms were found to occupy only octahedral positions. Zn atoms were also found to occupy both tetrahedral and octahedral sites.

In this work, we investigated the effects of ZrO₂ content on the microstructure and the electrical characteristics of the BaO-TiO₂ system. X-ray powder diffraction (XRD), scanning electron microscopy (SEM), DTA and standard electrical measurement procedures were used.

MATERIALS AND METHODS

Reagent grade raw materials were used in compositions suggested, thus BaO, ZrO₂ and TiO₂ chemical grade oxides were used. Two groups of mixes were suggested to study the electrical properties of semiconductor (BaO, TiO₂ and ZrO₂) according to Table 1 and Fig. 1. The prepared BaO, ZrO₂ and TiO₂ was wet grounded in a ball for a period of 3 hour to pass 200 mesh sieves. The slurry was dried overnight and used to fulfill the above-mentioned mixes. The mixes were weighed in the suggested proportions, wet milled to ensure thorough mixing of the different compositions then dried at 110°C. Two discs were used, the first one has 1.2 cm diameter and 0.2 cm thickness and the second disc has 5 cm diameter and 0.2 cm thickness. These two discs were processed by a semi-dry press method under 70 KN. Small specimens were subjected to thermal treatment to select the proper maturing temperature for each mix. Three discs were always fired in muffle kiln with a rate of heating of 5 °C/ min in the temperature range between (900 -1200)°C and for hours. The starting materials namely; BaO, ZrO₂ and TiO₂ were examined by XRD. Using Philips apparatus type 170, a vanadium ($\lambda=1.54 \text{ \AA}$) and Ni-filter. A continuous plot of intensity for 2θ values 4 to 80 was made at a scanning speed of 1°/ minute, with a paper speed of 10 mm/min.

The V - I characteristics of samples were measured at room temperature with a high - voltage source measure unit (Keithley237). The dielectric constant, resistivity and conductivity were measured at room temperature with change of frequency (1 - 20) kHz using RCL meter (PM 6304 programmable automatic).

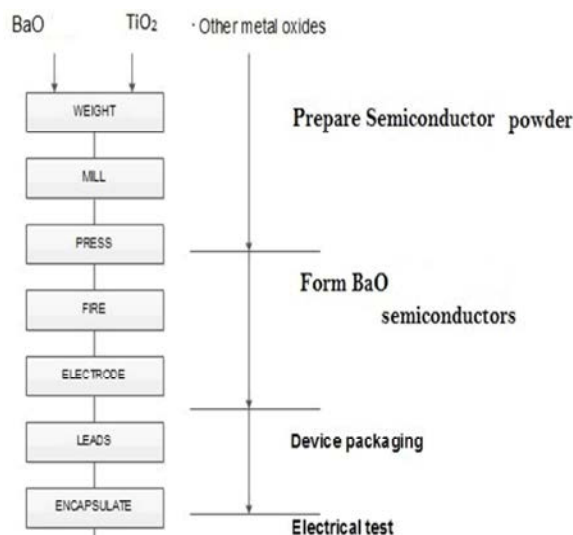


Fig. 1: Simplified flow diagram for the fabrication of BaO semiconductors.

Table 1: Composition of different mixes in mol%

Oxide Mixes	N0	N1	N2	N3	N4	N5
BaO	99	99	99	99	99	99
ZrO ₂	0.1	0.2	0.25	0.35	0.4	0.5
TiO ₂	0.9	0.8	0.75	0.65	0.6	0.5

The microstructures of samples were examined via the scanning electron microscopy (SEM, Joel - JEM.T200). DTA locates the ranges corresponding to the thermal decomposition of different Phases in paste, while TG measures the weight loss due to the decomposition. TG coupled with DTA makes it possible for the hydration reaction to be followed qualitatively, semi-qualitatively and quantitatively.

RESULTS AND DISCUSSION

Results of XRD patterns of different mixes are present in Fig. 2. It is evident that the main peaks present correspond to the contributing oxides namely [Barium oxide (BaO), Zirconium oxide (ZrO₂) and Titanium oxide (TiO₂)] and other different compounds. In all Figures, we find that the structure has a single phase with shift in the position of peaks (change in d-spacing). Some of peaks are not present, this may be attributed to the prefer orientation and has been happened between different oxides. Fig. 2 shows the X-ray diffraction pattern of N₀ annealed at 560°C for 10 min in oxygen atmosphere in which, Barium peroxide BaO₂, tetragonal phase (a=3.81140, b=3.81140 and c=6.82150), at about $2\theta=26.077$

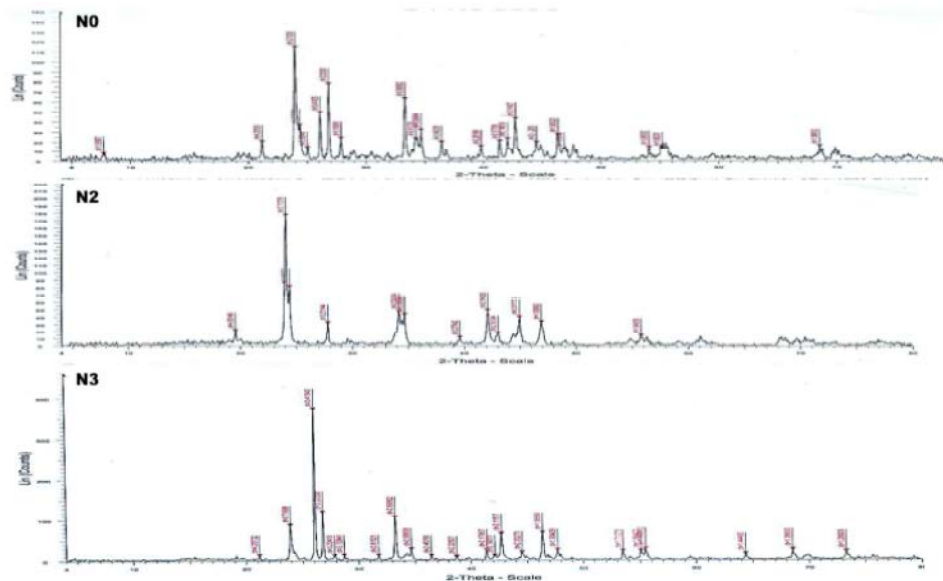


Fig. 2: XRD of different mixes [BaO, ZrO₂, TiO₂]

$d=3.414350 \text{ \AA}$, $2\theta=36.461^\circ$ $d=3.32292 \text{ \AA}$, $2\theta=34.674^\circ$ $d=2.68902 \text{ \AA}$, $2\theta=42.733^\circ$ $d=2.11427 \text{ \AA}$, $2\theta=46.403^\circ$ $d=1.95523 \text{ \AA}$, $2\theta=68.646^\circ$ $d=1.36612 \text{ \AA}$, the diffraction peaks at $2\theta=23.95^\circ$ $d=3.71225 \text{ \AA}$, $2\theta=34.674^\circ$ $d=2.58494 \text{ \AA}$. Corresponds to BaCO₃, witherite, (orthorhombic $a=5.31260$ - $b=8.89580$ $c=6.42840$).

Also Fig. 2 shows the X-ray diffraction pattern of sample N₃ annealed at 560°C for 10 min in oxygen atmosphere, in which BaCO₃, witherite (orthorhombic phase, $a=5.31260$ - $b=8.89580$ $c=6.42840$) at about $2\theta=26.069^\circ$ $d=3.41543 \text{ \AA}$, $2\theta=33.272^\circ$ $d=2.69062 \text{ \AA}$. Barium peroxide (tetragonal phase, $a=3.81140$ - $b=3.81140$ - $c=6.82150$) at about $2\theta=26.069^\circ$ $d=3.41543 \text{ \AA}$, $2\theta=26.788^\circ$ $d=3.32536 \text{ \AA}$ $2\theta=33.272^\circ$ $d=2.69062 \text{ \AA}$, $2\theta=42.714^\circ$ $d=2.11517 \text{ \AA}$, $2\theta=46.394^\circ$ $d=1.95559 \text{ \AA}$, the diffraction peaks at $2\theta=21.099^\circ$ $d=4.20732 \text{ \AA}$, $2\theta=23.908^\circ$ $d=3.71898 \text{ \AA}$, $2\theta=26.788^\circ$ $d=3.32636 \text{ \AA}$. Corresponds to Zirconium oxide Zr_{0.95}O₂ (tetragonal phase $a=5.15297$ - $b=5.15297$ - $c=5.28172$). From all patterns, three phases are identified, BaO₂ phase - TiO₂ phase and ZrO₂ phase. There are additional peaks are present BaCO₃ and there intensity increases with increasing TiO₂. The absent of some peaks of other oxides due to the formation liquid phase at low temperature. The absent of any diffraction line of TiO₂, ZrO₂ present in BaO can be attributed to a complete dissolution of this dopants oxides in the lattice of BaO and forming solid solution.

Fig. 3 shows the differential thermal analysis (DTA) thermogram of sample N₀ that contains 98.54 wt% BaO, 0.079 wt% ZrO₂ and 1.378 wt% TiO₂. The thermogram

shows endothermic effect in which, the onset point of the peak at 83.56 °C, the peak 1 top at 103.01 °C, the offset 2 at 104.07 °C, and enthalpy /μv.s/mg is 21.557. In addition to endothermic effect in which, onset point 124.17 °C, the peak 1 top at 127.18 °C, the offset at 127.56 °C, enthalpy/μv.s/mg is 0.11979, the onset point is 316.31 °C, the peak one top is 318.48 °C, the peak two top is 318.48 °C, Enthalpy/μv.s/mg is 0.0957, the onset point is 328.18 °C, the peak one top is 332.3 °C, the peak two top is 333.09 °C, Enthalpy/μv.s/mg is 0.1052, the onset point is 349.39 °C, peak 1 top is 353.91 °C, peak 2 top is 354.27 °C, Enthalpy/μv.s/mg is 0.490, the onset point is 361.59 °C, peak 1 top is 370.43 °C, peak 2 top at 372.56 °C, Enthalpy/μv.s/mg is 1.8561, the onset point is 443.41 °C, peak 1 top at 450.70 °C, peak 2 top 452.07 °C, enthalpy/μv.s/mg is 0.271, onset point is 477.41 °C, peak 1 top at 483.81 °C, peak 2 top at 452.07 °C enthalpy/μv.s/mg is 0.2747 and exothermic effect, in which the onset point is 477.41 °C, peak 1 top at 483.81 °C, peak 2 top at 489.16 °C and Enthalpy /μv.s/mg is -0.6497.

Fig. 3 shows DTA thermogram of sample N₃, which contains 98.833 wt% BaO, 0.401 wt% ZrO₂, and 0.769 wt% TiO₂. The thermogram reveals four endothermic effects, in which the onset point 63.88 °C, the peak 1 top at 91.23 °C, the offset top at 93.94 °C, enthalpy/μv.s/mg is 3.4928, the onset point 108.20 °C, the peak 1 top at 110.49 °C, the offset top at 111.13 °C, enthalpy/μv.s/mg is (0.0822), the onset point 299.14 °C, the peak 1 top at 306.80 °C, the offset top at 306.92 °C, enthalpy/μv.s/mg is (1.1951), the onset point 472.41 °C, the peak 1 top at 480.81

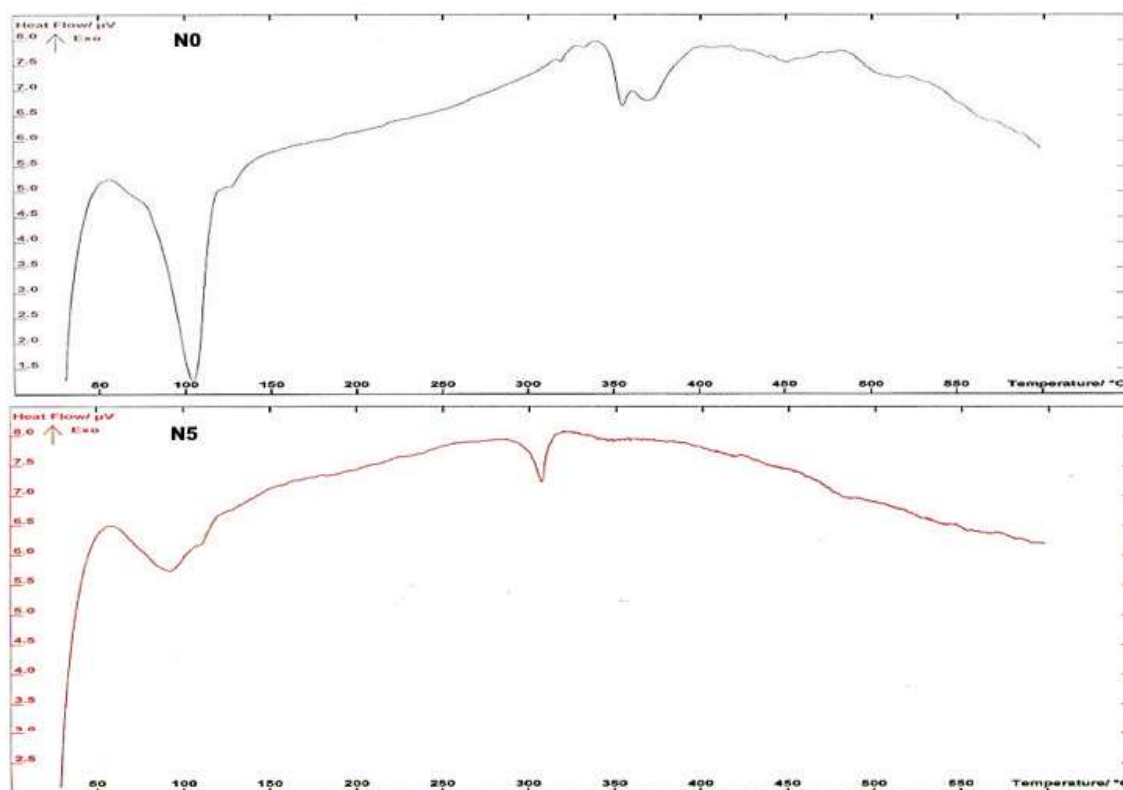


Fig. 3: The DTA of mix N0 and N5 [BaO, ZrO₂, TiO₂]

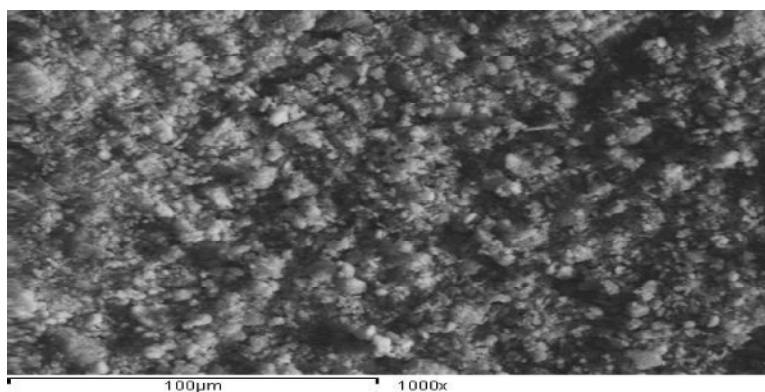


Fig. 4: SEM of mix N₀, thermally etched, shows of solid solution of BaO and ZrO₂ X=1000

°C, the offset top at 481.55°C, enthalpy /μv.s/mg is 0.1915. SEM of disc specimens fired at selected maturing temperature and thermal etched at 560°C for 10 min different mixes are demonstrated in Figs. 4-6.

The SEM of mix (N₀) containing BaO 0.079mol% ZrO₂ and 1.378 mol% TiO₂ presented in Fig (4), showed BaO agglomerates of various size and shapes, some of these agglomerates are deselected and fine grains are incorporated. The SEM of mix (N₁), containing BaO, 0.16mol% ZrO₂ and 1.228 mol% TiO₂ present in Fig. (5),

showed a homogeneous primary particle size of 1-3 μm, BaO grains dissolution of ZrO₂ between BaO grains. The SEM of mix N₃, containing BaO, 0.28 mol% ZrO₂ and 0.999 mol% TiO₂ present in Fig. (6), shows liquid phase in the triple point appears as white spots. BaO grains are tend together and growing in size and presence of pores of various size indicating a kind of volatilization, Zr, Ti go into solid solution in the BaO grains also a micro crack with irregular shape was observed. The x1000 sample shown unclear grains with low density. BaTiO₃ has high

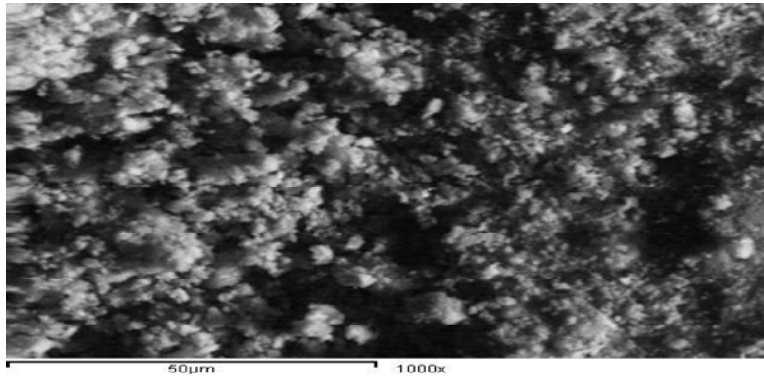


Fig. 5: SEM of (N₁), Thermally etched, shows a mass of solid solution of BaO and ZrO₂, X=1000.

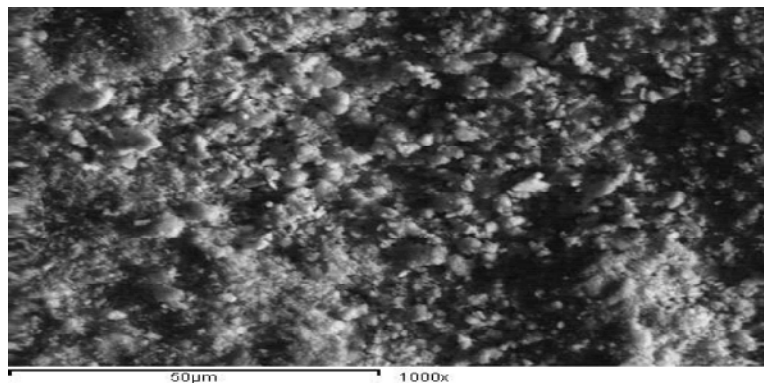


Fig. 6: SEM of mix (N₃), Thermally etched, show liquid phase X=1000.

relative permittivity, a large number of samples and complex oxides with perovskite structure of a general formula ABO_3 (A= mono or divalent, B= tri-hexavalent ions) have been examined to search for ferroelectric properties that have wide range of applications [28-30]. Ba (Ti_{0.8} Zr_{0.2})O₃ (BTZ) have found extensive application in optical devices, capacitors, etc [31-32].

Semiconductors based on barium titanate are frequently used in making multilayer capacitors. The rare earth cations which, partly replace the original cation in the spinel structure of (BZT) can increase the dielectric properties and prolong the life-span of capacitors. Doping of rare earth elements such as Dy, Er and Ho with smaller radius can obtain the centre-shell structure, which is helpful to improve the dielectric properties [33, 34], whereas doping of rare earth elements such as La with large ionic radius cannot improve the dielectric properties. HaO et al reported that Er is better than of Dy in improving the dielectric properties of BaZrTiO semiconductors [35]. Most of the solid ionic compounds are poor ionic conductors; only a few of them exhibit considerable ionic conductivity at elevated temperatures. The ionic conductors have various types of skeleton structure [36], which provide a pathway for mobile ions. Among the

three dimensional skeleton structure types, pyrochlores offer interesting possibilities as fast ion conductors. Although pyrochlores known for active and passive electronic applications, such as switching elements, thermistors, thick-film resistors, screen printing material for quite sometimes, they have been recognized only recently as potential candidates for temperature-stable, low-loss, high permittivity dielectric applications [37-39].

In addition to these promising properties and applications, the $R_2(M'M'')O_7$ (R=lanthanides, M'=alkaline and M''=W, Mo) system can be sintered at very low temperature, which makes them viable as co-fired dielectric components. Pyrochlore is a superstructure of the fluorite structure-type AB_2 , with the A- and B-site cations are ordered and one eighth of the anions are missing [37, 38]. Most of the pyrochlores have III-IV compositions with a formula $A_2^{3+}B_2^{4+}O_7$. Some Pyrochlore compounds are intrinsic oxide conductor and are useful for solid electrolytes in fuel cells [39]. The dielectric parameters (i.e., ϵ' and $\tan\delta$) of NBM= $Nd_2(Ba_{0.5}Mo_{0.5})_2O_2$ and NBW= $Nd_2(Ba_{0.5}W_{0.5})_2O_2$ at room temperature decrease on increasing frequency indicating a normal behavior of dielectric materials having mobile charge carriers (i.e., ions and electrons) [40].

Table 2: Variation of dielectric constant (ϵ') with frequency (kHz) at constant temperature of group (I)

Freq kHz	Sample					
	N ₀	N ₁	N ₂	N ₃	N ₄	N ₅
1	113.809	291.18	480.4059	568.909	175.3444	436.0726
2	58.1465	78.256	383.5741	469.186	93.3382	174.7207
3	38.5847	38.032	217.0534	210.755	44.0916	78.3114
4	29.4366	23.685	141.9599	122.38	26.0683	49.6749
5	23.6634	16.924	63.654	75.6583	18.0657	34.803
6	19.781	13.282	56.5978	56.2164	13.474	23.148
7	18.1903	11.682	40.3091	46.004	11.47101	18.529
8	16.095	10.262	29.96031	36.5907	9.6799	15.5
9	14.431	9.0058	28.4265	28.368	8.10708	13.5205
10	12.645	7.9267	22.6031	21.1178	6.7295	9.5088
20	7.5416	5.6062	15.0502	15.4877	3.8214	3.0625
30	6.9208	5.2175	8.4777	10.1145	3.3149	1.5988

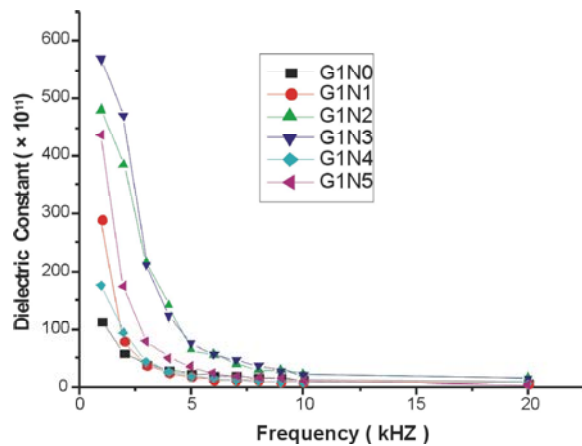


Fig. 7: Effect of frequency (kHz) on Dielectric constant of different mixes

At low frequencies (102-104 Hz), normally all types of polarizations exist [41]. However, in the case of NBM and NBW, the ionic and electronic polarization exists at the high-frequency range. The relation between dielectric constant (ϵ') and frequency in kHz for the mixes of different compositions is presented in Fig. 7. The experimental data shown in Table 2 and Fig. 7 reveal conclusively that the dielectric constants of different mixes are strongly dependent on the frequency and contents of ZrO_2 and TiO_2 . The dielectric constant decreases as the content of ZrO_2 increases from 0.079 mol% to 0.401 mol%, reaches a minimum value (1.5988) at 30 kHz in sample N₅. It was also observed that there is an obvious decrease in the value of the dielectric constant with increasing frequencies up to 20 kHz at room temperature, which can be attributed to the absence of the space charge polarization at these frequencies.

At higher frequencies (>20 kHz), there is an increase in the dielectric constant, which is due to the resonance phenomenon [42].

The general trend for all composition is that capacitance (pf) and dielectric constant (ϵ') decrease with increasing frequency. This behavior of a dielectric may be explained qualitatively by the supposition that the mechanism of the polarization process in BaTiO_3 and ferrite is similar to that the conduction process. The electrical conduction mechanism can be explained by the electron-hopping model of Heikes and Johnston [43]. In general, the decrease of capacitance in (pf), dielectric constant (ϵ') and consequently increase (AC) conductivity with increasing frequency (1 -20) kHz. This behavior reflects the transition from one process to another process, which may be related to a thermally activated charged particle in accordance with Maxwell - Wagner mechanism [44, 45]. This results in a monotonous decrease in the value of dielectric constant on increasing frequency for all the concentration. This observation may be attributed to a combined contribution to the dielectric constant due to electric, ionic, interfacial polarization at low frequencies.

CONCLUSIONS

Donor doped BaTiO_3 ceramics introduced n-type semiconductor characteristic and exhibit a positive temperature coefficient of resistivity (PTCR). Intergranular barrier layers at the grain boundaries govern the electrical properties in BaTiO_3 based ceramics. In polycrystalline semiconductors, the trapping of charge at the grain boundaries has a decisive influence on the electrical transport properties by means of the formation of electrostatic potential barriers.

The DTA pattern shows a clear indication of two maxima occurring at the point 112°C and 210°C, respectively. This may be interpreted to be the beginning of mass due to release of surface adsorbed water content and initiation of the intermediate reaction steps. A small hump at 550°C in the DTA pattern may be related to the evolution of gases towards the end of the reaction when the mass loss attains saturation limit. The SEM of different mixes shows BaO grains are tend together and growing in size and presence of pores of various size indicating a kind of volatilization, also Zr, Ti go into solid solution in the BaO grains. The relation between conductivity and frequency of different mixes at constant temperature show the decrease of capacitance in (pf), dielectric constant (ϵ') and consequently increase (AC) conductivity with increasing frequency (1 - 20) kHz. In general, the decrease of capacitance in (pf), dielectric constant (ϵ') and consequently increase (AC) conductivity with increasing frequency (1 - 20) kHz. This behavior reflects the transition from one process to another process, which may be related to a thermally activated charged particle in accordance with Maxwell - Wagner mechanism.

REFERENCE

- Mastai, Y., Y. Diamant, S.T. Aruna and A. Zaban, 2001. *Langmuir*, 17: 711.
- Tian, Z.R., W. Tong, J.Y. Wang, N.G. Duan, V.V. Krishnan and S.L. Suib, 1977. *Science*, 276: 926.
- Nakade, S., Y. Saito, W. Kubo, T. Kitamura, Y. Wada and S. Yanagida, 2003. *J. Phys. Chem. B* 107: 860.
- Karch, J., R. Birringer and H. Gleiter, 1987. *Nature*, 330: 556.
- Yin, J.B. and X.P. Zhao, 2002. *Chem. Mater.*, 14: 4633.
- Zhu, Y., J. Shi, Z. Zhang, C. Zhang and X. Zhang, 2002. *Anal. Chem.*, 74: 120.
- Gratzel, M., 1992. *Nature*, 353: 737.
- Hoffmann, M.R., S.T. Martin, W. Choi and D.W. Bahnemann, 1995. *Chem. Res.*, 95: 69.
- Hsu, J.P. and A. Nacu, 2003. *Langmuir*, 19: 4448.
- Zhang, Q. and L. Gao, 2003. *Langmuir*, 19: 967.
- Lim, K.T., H.S. Hwang, W. Ryoo and K.P. Johnston, 2004. *Langmuir*, 20: 2466.
- Karuppuchamy, S., K. Nonomura, T. Yoshida, T. Sugiura and H. Minoura, 2002. *Solid State Ionics*, 151: 19.
- Pradhan, S.K., P.J. Reucroft, F.Q. Yang, A. Dozier and J. Cryst., 2003. *Growth*, 256: 83.
- Neiman, S.M., 1988. *J. Mater. Sci.*, 23: 3973.
- Fang, T.T. and P.H. WU, 2002. *Mater. Chem. Phys.*, 72: 346.
- Hennings, D., A. Schnell and G. Simon, 1982. *J. Am. Ceram. Soc.*, 65: 539.
- Rehrig, P.W., S.E. Park, S.T. rolter-MsKinstry, G.L. Messing, B. Jones and T.R. Shrout, 1999. *J. Appl. Phys.*, 86: 1657.
- Yu, Z., R. Guo and A.S. Bhalla, 2000. *Appl. Phys. Lett.*, 77: 153.
- Yu, Z., R. Guo and A.S. Bhalla, 2000. *J. Appl. Phys.*, 88: 410.
- Hofer, C., M. Hoffmann, U. Boettger and R. Waser, 2002. *Ferroelectrics*, 270: 1365.
- Kamehara, N., M.T. Sukada, J.S. Cross and K. Kurihara, 1997. *J. Ceram. Soc. Jpn.*, 105: 746.
- Halder, S., S. Bhattacharyya and S.B. Krupanidhi, 2002. *Mater. Sci. Eng., B*, 95: 124.
- Mizuno, F. and M. Sato, 1993. US patent 5,272,122.
- Dielectric Resonators, Murata Cat. No. O95E-8.
- Gornikov, Yu. I., Z. Ya. Makarova, A.G. Belous, L.G. Gavrilova, V.M. Paskov and V.P. Chalyi, 1984. *Sov. Prog. Chem.*, 12(50): 1243-1245.
- Negas, T., 1993. Trans Tech Inc., US patent, 5262, 370.
- Roth, R.S., C.J. Rawn, C.G. Lindsay and W. Wong-Ng, 1993. *J. Solid State Chem.*, 104: 99-118.
- Zimmermann, F., M. Voigts and W. Menesklou, 2004. *J. Eur. Ceram. Soc.*, 24: 1729.
- Hao, S.E. and Y.D. Wei, 2003. *J. Inorg. Mater.*, 18: 1069 (in Chinese).
- Kumazawa, H. and K. Masuda, 1999. *Thin Solid Films*, 353: 144.
- Reymond, V., S. Payan and D. Michau, 2004. *Thin Solid Films*, 467: 54.
- Jeon, H.P., S.K. Lee, S.W. Kim and D.K. Choi, 2005. *Mater. Chem. Phys.*, 94: 185.
- Watanabe, K. and H. Ohsato, 1998. *Solid State Ionics*, 108: 129.
- Stojanovic, B.D., C.R. Fosochini and M.A. Zahete, 2003. *J. Mater. Process. Tech.*, 143: 802.
- Hao, S.E., L. Sun and J.X. Huang, 2008. *Materials Chemistry and Physics*, 109: 45-49.
- Goodenough, J.B., H.Y.P. Hong and J.A. Kafalas, 1976. *Mater. Res. Bull.*, 11: 203.
- Subramanian, M.A., G. Aravamudan and G.V.S. Rao, 1983. *Prog. Solid State Chem.*, 15: 55.
- Chakoumakes, B.C., 1984. *J. Solid State Chem.*, 53: 120.

39. Lian, J., L. Wang, J. Chen, K. Sun, R.C. Ewigy and L.A. Boatner, 2003. *Acta Mater*, 51: 1493.
40. Anderson, J.C., 1964. *Dielectrics*, Chapman & Hall, London.
41. Lidorenko, N.S, V.E. Zil'bervarg and E.L. Nagaer, 1980. *Sov. Phys. JETP*, 51(1): 89.
42. Mezahi, F., A. Harabi, S. Zouai, S. Achour and D. Bernache-Assollant, 2005. *Mater. Sci. Forum.*, pp: 492-493.
43. Heikes, R.R. and D. Johnston, 1957. *J. Chem. Phys.*, 26: 582.
44. Lee, K.S.J., 1996. *Phys. chem. Solid*, 57: 333.
45. Ortiz, E., R.A. Vargas and B.E. Mellander, 1998. *J. phys. chem. Solids*, 59: 305.